Indian Journal of Chemical Technology
Vol. 29, July 2022, pp. 402-411

Synergistic corrosion inhibitor of carbon steel by dihydroxy benzyl phosphonic acid -Zn^{2+} system in O.5 M H_2SO_4: Experimental and theoretical studies

Rachida Kerkour*[,1,2], Ouahiba Moumeni[1], Meriem Djenane[1] , Nadjib Chafai[1] & Saleh Chafaa[1]

[1]Laboratory of Electrochemistry of Molecular Materials and Complex (LEMMC), Department of Process Engineering, Faculty of Technology, University of Ferhat Abbas Sétif-1, El Maabouda 19000 Setif, Algeria

[2]Department of Science and Technology, Institute of Science and Technology, University of Abdelhafidh Boussouf, Mila, Algeria

E-mail: labiba@univ-sétif.dz

Received 17 September 2021; accepted 24 May 2022

The synergistic effect of dihydroxy benzyl phosphonic acid (DAP) and zinc sulfate $ZnSO_4$ (Zn^{2+}) system in 0.5 M H_2SO_4 solution on carbon steel X48 has been evaluated using potentiodynamic polarization measurements, electrochemical impedance spectroscopy (EIS), scanning electron microscope (SEM), and quantum methods (DFT). The combination of DPA and Zn^{2+} has been demonstrated to have remarkable inhibitory efficiency (96%). DPA/Zn^{2+} formulation operate as a mixed inhibitor, inhibiting both the anodic and cathodic reactions to the same amount, according to polarization studies. The diameter of the semicircles increases with the addition of DPA/Zn^{2+} formulation. Furthermore, the double layer capacitance C_{dl} decreases and R_t values increase with this combination of DPA and Zn^{2+}, confirming the significant adsorption on the surface steel. The adsorption isotherm of Langmuir is approached by the adsorption on the metal surface. The nature of the protective coating is also determined using surface characterization techniques (FTIR and SEM). The molecular orbital (HOMO and LUMO) energies, energy gap (ΔEgap), dipole moment (μ), global hardness (η), global softness (σ), electrophilicity index (ω), absolute electronegativity (χ) and the fraction of transferred electrons (ΔN) have been determined as supporting evidence.

Keywords: Corrosion inhibition, DFT, FTIR, Phosphonic Acid, SEM, Synergistic effect, XC48

Carbon steel is the most frequently used material, accounting for approximately 85% of yearly steel production worldwide. Marine applications, nuclear power, fossil fuel power plants, petroleum production, chemical processing, refining, construction, and metal-processing equipment all use huge amounts of carbon steel. Carbon steel, on the other hand, has a significant disadvantage in terms of corrosion resistance in hostile conditions[1-4].

So far, adding organic molecules to acid media has been one of the most prevalent, effective, and cost-effective methods of protecting metals. The existence of polar functionalities with nitrogen, sulfur, or oxygen atoms in the molecule affects the inhibitor's efficacy[5,6]. The phosphonic acids have received a lot of attention and have been utilized as inhibitors; however, they do not create any noticeable modifications in general corrosion behaviour[-7-10]. Studies have been conducted to investigate synergistic effects of other additives in order to improve the latter's performance. Several writers have looked into the synergistic effect that phosphonic acids and Zn^{2+} have on metal corrosion inhibition[11-15]. The aim of the present work was to investigate the synergistic effect of DAP and zinc on the corrosion inhibition efficiency of carbon steel in sulfuric acid, using potentiodynamic polarization curves, electrochemical impedance measurements (EIS). Fourier transform infrared (FTIR) spectroscopy and scanning electron microscopy (SEM) were also used to characterize the surface. The absorption sites were assigned using quantum chemical calculations using DFT (B3LYP) methods with the basis set 6–31G(d,p).

Experimental Section

Material preparation

All experiments were performed using carbon steel specimen X48 of the following composition: (wt. percent C: 0.50; Mn: 0.80; Si: 0.40; Mo: 0.10; Ni: 0.40; Cr: 0.40; P: 0.045; S: 0.05 and Fe: 0.05). (remainder), the working electrode was as disk with surface area of 0.2 cm^2 that was exposed to the corrosive solution . The specimen was polished with a series of emery papers (400, 600, 1000 and finally 4000 grade) then degreased with methanol and finally washed thoroughly with distilled water. The aggressive solution of 0.5 M H_2SO_4

was prepared by the dilution of an analytical reagent grade 98% H_2SO_4 (Sigma-Aldrich) and distilled water. Doses of the utilized inhibitor ranged from 1×10^{-6} to 1×10^{-3} mol L^{-1}. The experiments were all carried out at room temperature.

Inhibitor preparation

The test inhibitor was the dihydroxy benzyl phosphonic acid (DPA), which was synthesized in the laboratory using a process previously described[16]. Doses of the utilized inhibitor ranged from 1×10^{-6} to 1×10^{-3} mol L^{-1} in H_2SO_4 solution. In the form of zinc sulfate solution, Zn^{2+} ions were added to the DAP.

Electrochemical measurement

The corrosion behavior was studied using electrochemical measurement techniques such as DC-Tafel slope and AC-Electrochemical impedance Spectroscopy (EIS). Electrochemical experiments were carried out utilizing a three-electrode setup. The reference electrode was a saturated calomel electrode (SCE), the counter electrode was a platinum disk with a surface area of 2 cm^2, and the working electrode was a carbon steel disk with a surface area of 0.2 cm^2. A PGZ 301 Volta lab 40 system was used for all of the tests. To establish a steady state open circuit voltage, the working electrode was immersed in the test solution for 30 minutes.

Polarization measurements were taken at a scan rate of 0.5mV/s from -0.8 to -0.2V. To calculate the corrosion current density(i_{corr}), the linear Tafel segments were extrapolated to E_{corr}. The inhibition efficiency (IE) was calculated from the measured i_{corr} using the following formula[17].

$$IE(\%) = \frac{(i^{\circ}_{corr} - i_{corr})}{i^{\circ}_{corr}} \times 100 \quad ...(1)$$

where i_{corr} and i^{o}_{corr} are the inhibited and uninhibited corrosion current densities, respectively.

The electrochemical impedance spectroscopy (EIS) measurements were performed at an open circuit potential with a frequency range of 100 KHz to 10 mHz and a 10 mV amplitude. The diameter of the semicircle in Nyquist representation was used to calculate the charge transfer resistance (R_{ct}). The following formula[17] was used to calculate the inhibitor's inhibitory efficiency (IE).

$$IE(\%) = \frac{R_{inh} - R_t}{R_{inh}} \times 100 \quad ...(2)$$

where R_t and R_{inh} are the charge transfer-resistance values without and with inhibitor, respectively.

Surface examination study

For one day, the carbon steel specimens were immersed in various test solutions. The specimens were then removed, properly cleaned with water, and dried. Various surface analysis techniques were used to investigate the nature of the film produced on the metal specimens' surfaces. On a JASCO 4200 spectrometer, FT-IR spectra in the range of 4000 and 200 cm^{-1} were acquired. A computer-controlled scanning electron microscope (JOEL-JSM-7001F-Japan) was used to evaluate scanning electron microscopic studies (SEM) of carbon steel samples.

Theoretical studies

On the basis of a set of functions, the conceptual density functional theory provides a point of view for understanding and forecasting experimental and theoretical stability and reactivity[18]. Many investigations on corrosion inhibitors have lately been undertaken[19,20]. Theoretical calculations were carried out utilizing the Gaussian 03 program package and the Beck's three parameter exchange functional, as well as the Lee–Yang–Parr nonlocal correlation functional (RB3LYP) using the 6-31G (d, p) basis set[21]. The E_{HOMO} and E_{LUMO} energies (highest occupied molecular orbital energy and lowest unoccupied molecular orbital energy) were used to calculate all the quantum chemical parameters such as energy gap (ΔEgap), dipole moment (μ), global hardness (η), global softness (σ), electrophilicity index (ω), absolute electronegativity (χ) and the fraction of transferred electrons (ΔN) using the following equations[22-24] and the results were visualized by means of Gauss View 5.0.8 computer software[25].

$$\eta = \frac{E_{LUMO} - E_{HOMO}}{2} \quad ...(3)$$

$$\sigma = \frac{1}{\eta} \quad ... (4)$$

$$\omega = \left(\frac{\chi^2}{2\eta}\right) \quad ...(5)$$

$$\chi = \frac{-(E_{HOMO} + E_{LUMO})}{2} \quad ...(6)$$

$$\Delta N = \frac{\chi_{Fe} - \chi_{inh}}{2(\eta_{Fe} + \eta_{inh})} \quad ...(7)$$

Results and Discussion

Polarization measurements

Figures 1(a) and 1(b) depicts the potentiodynamic polarization behaviour of carbon steel in 0.5 M H_2SO_4 with and without various doses of DAP and DAP/Zn^{2+} system. Table 1 lists electrochemical characteristics

determined from polarization curves, such as corrosion densities (i_{corr}), corrosion potential (E_{corr}), cathodic Tafel slope (β_c), and anodic Tafel slope (β_a). Corrosion current density (i_{corr}) in acidic media reduces noticeably as inhibitor concentration rises. On the other hand, at 298°C, the corrosion rate of carbon steel is lowered to the maximum value of 96.14 % for 10^{-3} DPA / Zn^{2+}. It is obvious that as the inhibitor concentration is increased, the corrosion inhibition improves. This is owing to the fact that when the inhibitor concentration rises, so does the quantity of adsorption and coverage of the inhibitor on the steel surface[26]. These findings also support the idea that DAP and Zn^{2+} ions work together to suppress carbon steel corrosion in H_2SO_4 solutions.

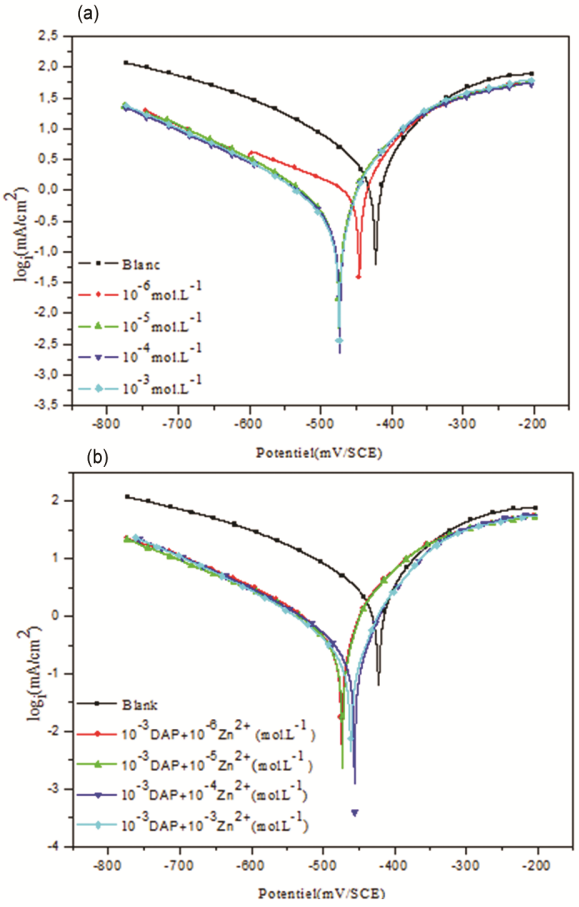

Fig. 1 — (a) Polarization curves for XC48 in 0.5 mol.L^{-1} H_2SO_4 with various DAP concentrations and (b) Polarization curves for XC48 in 0.5 mol.L^{-1} H_2SO_4 with various DAP/Zn^{2+} concentrations

Electrochemical Impedance Spectroscopy (EIS)

Figures 2(a) and 2(b) show Nyquist plots for carbon steel electrodes exposed for 30 min at the free corrosion potential in 0.5 M H_2SO_4 with, without DAP and with combination of DAP/Zn^{2+}. Table 2 shows the impedance parameters calculated from Nyquist plots. The impedance diagrams are virtually semicircles in appearance, but not perfect semicircles; these circles are constructed with the inductive loop at high frequency, as shown in these plots. The iductive loop can be attributed to the charge-transfer reaction, which is based on direct electron transfer at the metal surface, electron conduction through the film surface[27], adsorption, species $FeSO_4$[28], or inhibitor species on the electrode surface [29]. The inductive loop is not observed on the Nyquist diagram for acidic solution alone. Furthermore, increasing the concentration of DAP with or without the addition of Zn^{2+} causes an increase in the size of the semicircle, showing that the corrosion process is inhibited. The charge transfer resistance-based inhibition efficiency was determined to be 94.26 percent. The addition of the inhibitor improves R_t values while decreasing C_{dl} values (Fig. 3).

The evolution of the C_{dl} as a function of the DAP inhibitor effectiveness and the DAP/Zn^{2+} system is shown in Fig. 4. According to the Helmotz model, the double layer capactance C_{dl} is given by the equation:

Table 1 — Potentiodynamical parameters for the corrosion of XC48 in 0.5 mol.L^{-1} H_2SO_4 solution in the absence and presence of DAP and DAP/ Zn^{2+}

Concentration (mol.L^{-1})		Tafel parameters				Inhibition efficiency
DPA	Zn^{2+}	E_{corr} (mV/SCE)	i_{corr} (mA/cm^2)	β_a (mV/decade)	$-\beta_c$ (mV/decade)	IE (%)
Blank	0	-422.5	1.636	61.8	102.7	-
DPA.10^{-6}	0	-445.4	0.6515	94.9	161.0	60.06
DPA.10^{-5}	0	-473.1	0.5917	68.3	184.6	63.83
DPA.10^{-4}	0	-474.2	0.5464	64.3	156.7	66.60
DPA.10^{-3}	0	-473.9	0.4295	56.8	148.8	73.74
DPA.10^{-3}	Zn^{2+}.10^{-6}	-474.4	0.222	37.1	88.5	86.43
DPA.10^{-3}	Zn^{2+}.10^{-5}	-473.1	0.210	36.3	82.0	87.16
DPA.10^{-3}	Zn^{2+}.10^{-4}	-456.0	0.151	41.1	82.6	90.77
DPA.10^{-3}	Zn^{2+}.10^{-3}	-461.3	0.063	30.6	39.1	96.14

$$C_{dl} = \frac{\varepsilon_0 - \varepsilon}{\delta} . S \quad \ldots(8)$$

where

- δ : The thikness of the deposit,
- S : The surface of the electrode
- ε_0 : The permiabittivity of the air
- ε : The medium dielectric constant

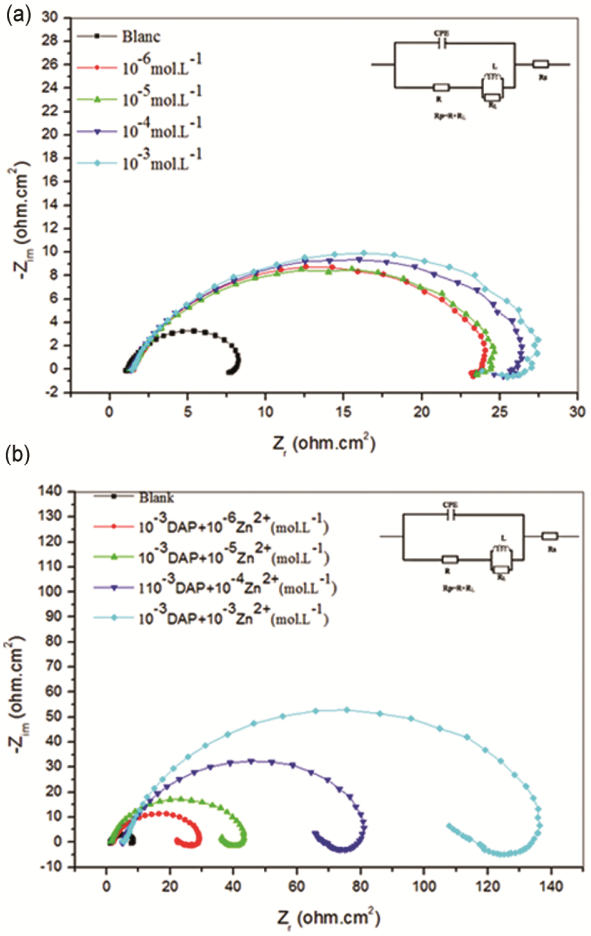

Fig. 2 — (a) Nyquist plots for XC48 steel in 0.5 mol.L^{-1} H_2SO_4 with and without DAP and (b) Nyquist plots for XC48 steel in 0.5 mol.L^{-1} H_2SO_4 with and without DAP /Zn^{2+}

The increase in R_t values can be attributed to the creation of a protective layer on the metal surface, resulting in an increase in surface coverage[30]. However, the decrease in C_{dl} values could be due to the inhibitor's adsorption on the surface of the metal, implying that the inhibitor works via adsorption at the metal-solution interface[31-33].

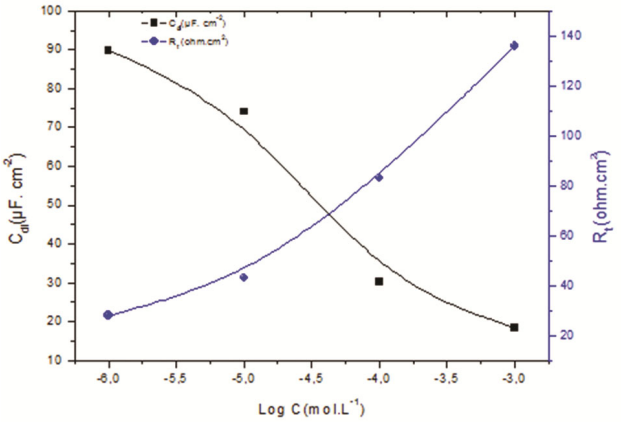

Fig. 3 — Evolution of transfer resistance and capacitance as a function of the logarithm of DAP/Zn^{2+} concentration

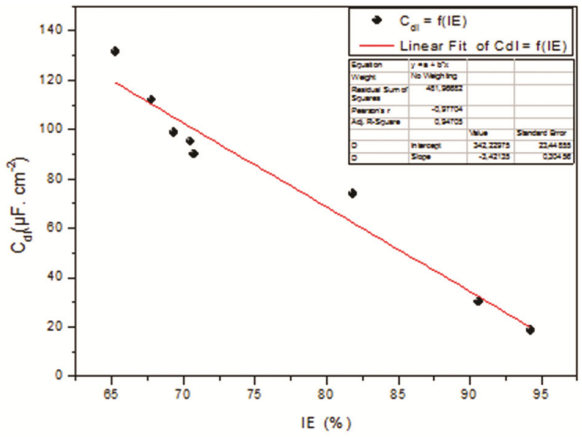

Fig. 4 — C_{dl} evolution in 0.5 mol.L^{-1} H_2SO_4 as a function of IE percent of XC48 steel with DAP and DAP/ Zn^{2+}

Table 2 — Impedance parameters of XC48 steel in mol.$L^{-1}$$H_2SO_4$ containing different concentrations of DPA and DPA / Zn^{2+}

Concentration (mol.L^{-1})		Impedance parameters			Inhibition efficiency
DPA	Zn^{2+}	R_s(Ω. m^2)	R_t (Ω.cm^2)	C_{dl}(µF. cm^{-2})	IE (%)
Blank	0	1.126	7.802	322.2	-
DPA.10^{-6}	0	1.664	22.45	131.4	65.24
DPA.10^{-5}	0	1.420	24.21	111.9	67.77
DPA.10^{-4}	0	1.536	25.46	98.76	69.35
DPA.10^{-3}	0	1.581	26.43	95.13	70.48
DPA.10^{-3}	Zn^{2+}.10^{-6}	1.073	27.98	89.86	70.74
DPA.10^{-3}	Zn^{2+}.10^{-5}	1.431	43.00	74.02	81.85
DPA.10^{-3}	Zn^{2+}.10^{-4}	1.451	83.02	30.28	90.60
DPA.10^{-3}	Zn^{2+}.10^{-3}	1.632	136.00	18.47	94.26

Adsorption isotherm

Adsorption isotherms are crucial in figuring out how organo electrochemical reactions work[34]. To explore the manner of adsorption, the following equation is used to calculate the surface coverage values (θ) for varied concentrations of DAP in the presence and absence of Zn^{2+}.

$$\theta = \frac{E(\%)}{100} \quad \text{... (9)}$$

The plots of C_{inh}/θ against C_{inh} for the inhibitor is shown in Fig. 5 and the equation 10 describes the relationship between and inhibitor concentration in corrosive medium.

$$\frac{C_{inh}}{\theta} = \frac{1}{K_{ads}} + C_{inh} \quad \text{...(10)}$$

K_{ads} is the related to the standard Gibbs free energy of adsorption ΔG_{ads}^{0}, it is expressed by equation 11, 55.5 is the molar concentration of water in the solution, R is the gas constant (8.314 $K^{-1}.mol^{-1}$) and T is the absolute temperature (K).

$$K_{ads} = \frac{1}{5.55}.e\left(\frac{\Delta G^{\circ}_{ads}}{RT}\right) \quad \text{...(11)}$$

The plots (Fig. 5), produces straight lines with linear regression and R^2 values of 0.9999. This validates the hypothesis that DAP and DAP/Zn^{2+} adsorption on a carbon steel surface follows the Langmuir adsorption isotherm[14]. Standard free energy values of -20 kJ mol^{-1} or less are associated with an electrostatic interaction between charged molecules and charged metal (physisorption), whereas those more negative than -40 kJ mol^{-1} are associated with charge sharing or transfer from inhibitor molecules to metal surface to form a coordinate covalent bond (chemisorption)[35,36]. Table 3 lists the parameter values obtained and calculated from the plot, as well as the derived $\Delta G°_{ads}$ values. For both potentiodynamic polarization and electrochemical impedance spectroscopy, the values were in the range of -39 to 43 kJ/mol, revealing that both physical adsorption and chemical adsorption[35,36].

We compared our results to those reported in previous research for similar types of compounds[37,38] to highlight the strong inhibition rate of the examined inhibitors (Table 4).

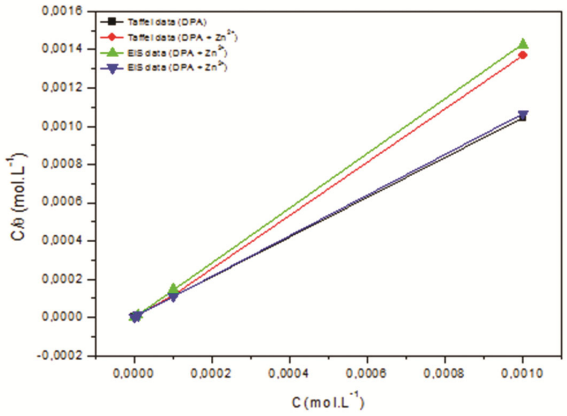

Fig. 5 — Langmuir adsorption isotherm model obtained by Tafel and EIS data for DAP and DAP/ Zn^{2+}

Table 3 — The parameters of the linear regression from the Langmuir adsorption isotherm for DAP and DAP+Zn^{2+} system

Method	Inhibitor	Slope	R^2	$K(Lg^{-1})$	ΔG_{ads}^{0} ($kJ.mol^{-1}$)
Potentiodynamic Polarization	DAP	1.374	0.99958	$1.636.10^5$	- 39.67
	DAP/Zn^{2+}	1.039	0.99994	$3.771.\ 10^5$	- 41.66
Impedance Spectroscopy	DAP	1.427	0.99998	$9.046.10^5$	- 43.91
	DAP/Zn^{2+}	1.061	0.99998	$4.435.10^5$	- 42.14

Table 4 — Comparison of the findings of this study with those of prior studies on comparable chemicals

	Inhibition Efficiency IE (%)		
	Present inhibitor	Prabakaran *et al.*[37]	Bouklah *et al.*[38]
Structure	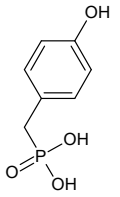	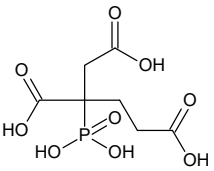	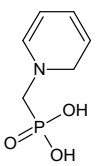
Weight loss method	-	96	88.8
Tafel method	96.14	81	89.7
Eis method	94.26	91	-

Fourier transform infrared spectroscopy (FTIR)

Figure 6 shows the FTIR spectrum of pure DAP and DAP / Zn^{2+} system. The P=O and P-OH stretching vibrations show at 1212.04 and 925.66-983.51 cm^{-1}, respectively, for pure DAP. However, the P-OH stretching has disappeared from the spectrum of the film formed on the metal surface after immersion in a solution containing 10^{-3} M DAP/Zn^{2+}, and the P=O stretching vibration shifts from 1212.04 to 1112.73 cm^{-1},

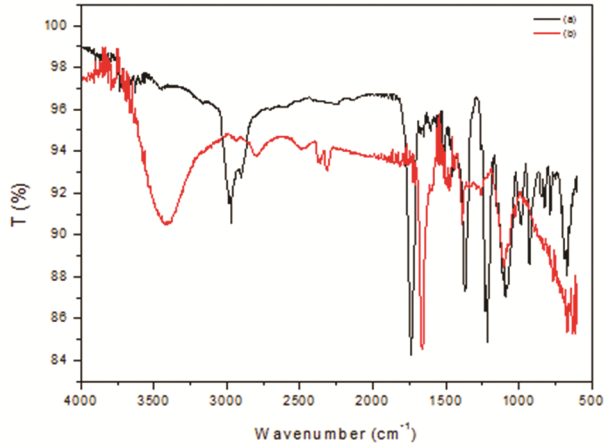

Fig. 6 — FTIR spectrum of pure (a) pure DAP and (b) DAP/Zn^{2+}

with an intense peak at 3412.42 cm^{-1} that can be attributed to the presence of an OH group on the carbon surface[39]. The signal at 1397.17cm^{-1} is due to Zn-O, indicating that $Zn(OH)_2$ was produced[39].

Scanning Electron Microscope (SEM)

Figure 7 shows SEM micrographs of carbon steel surfaces after 24 hours of immersion in the presence and absence of optimal concentrations of 10^{-3}M DAP and DAP/Zn^{2+} in 0.5M H_2SO4 solution. The SEM micrograph of a polished carbon steel surface (Fig.7a) reveals a uniform surface of carbon steel; nevertheless, after immersion in corrosive solution, certain cracks and pits occur on the metal's surface as a result of the corrosive solution's attack (Fig.7b). (Fig.7c) reveals that the surface created by the inhibition system has high inhibitive characteristics for carbon steel in acidic conditions, while the smoothness of the metal surface is revealed by the presence of 10^{-3}M DAP / Zn^{2+} [34].

Mechanism of corrosion inhibition

When carbon steel is immersed in an aqueous solution, the anodic and the cathodic reactions are:

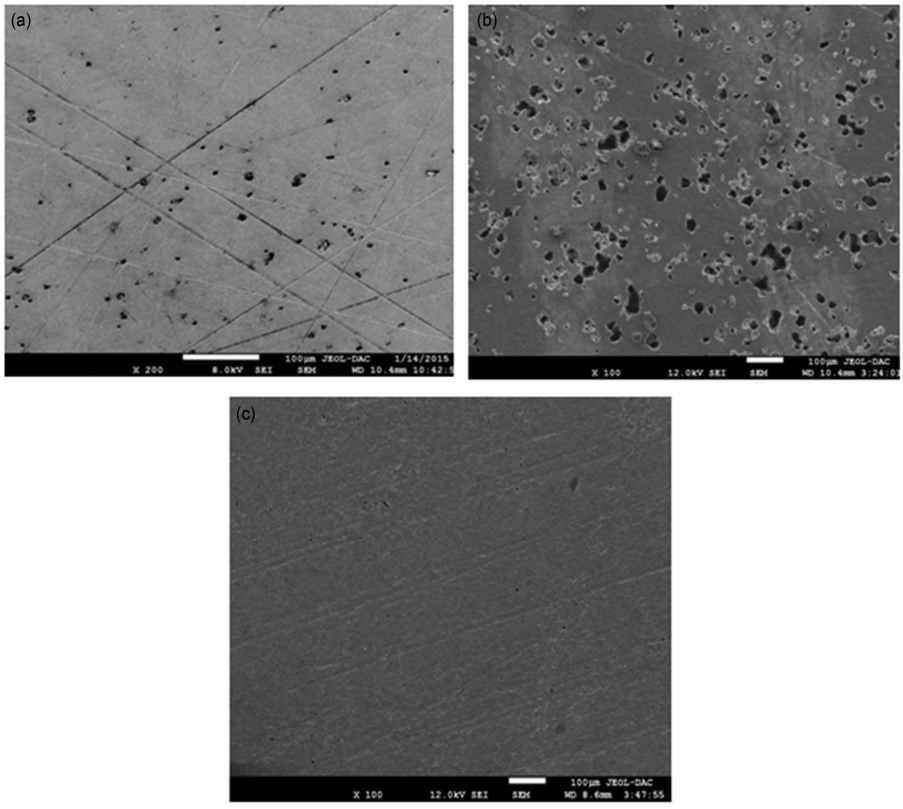

Fig. 7 — SEM micrographs of carbon steel surface; (a) Polished carbon steel (control); (b) After 24 h in 0.5 $mol.L^{-1}$ H_2SO_4 and (c) After 24 h in H_2SO_4 containing 10^{-3} M of (DAP / Zn^{2+})

$Fe \rightarrow Fe^{2+} + 2e^-$

$O_2 + 2H_2O + 4e^- \rightarrow 4OH^-$

When carbon steel is immersed in an acidic solution containing phosphonic acid, Fe^{2+} is produced, as well as a DAP-Fe^{2+} complex [40], and when carbon steel is immersed in this solution, the anodic reaction is controlled by the formation of DAP-$Fe^{2+}$and the cathodic reaction is controlled by the formation of $Zn(OH)_2$ on the cathodic sites. The following reactions are possible:

Zn^{2+} - DAP + $Fe^{2+} \rightarrow Fe^{2+}$ - DAP + Zn^{2+}

$Zn^{2+} + 2OH^- \rightarrow Zn(OH)_2$

As a result, the protective film is made up of a Fe^{2+}– DAP and $Zn(OH)_2$ complex, and FTIR analysis of the film confirmed this.

Synergism considerations of DAP with Zn ions

The synergistic inhibitory effect was calculated using the following equation and a parameter S_θ calculated from the surface coverage values (θ) of the anion, cation, and both.

where

$$S_\theta = \frac{1-\theta_{(1+2)}}{1-\theta'_{(1+2)}} \quad \ldots(12)$$

- $\theta_{1+2} = (\theta_1 + \theta_2) - (\theta_1\theta_2)$.
- θ_1 : Surface coverage by anion.
- θ_2 : Surface coverage by cation.
- θ'_{1+2} : Measured surface coverage by both the anion and cation.

The synergism parameter values for the various concentrations of the studied formulation were calculated using potentiodynamic polarization and impedance spectroscopy data, and the results are shown in Table 5. All of the calculated values are greater than unity, indicating that the corrosion inhibition caused by the DAP/Zn^{2+} system is synergistic and the results are in good agreement with what[41-43] has stated.

Theoretical studies

Some quantum chemical computations were performed after geometric optimization from DFT calculations, in order to inquire the relationship between the molecular structure and the inhibition efficiency of the studied compound, and the results are regrouped in Table 6.

Some researchers have previously reported that increased inhibition efficiency is caused by smaller values of ΔE_{gap} [44] and higher values of dipole moment μ[18]. Table 5 shows that the value of ΔE_{Gap} for DAP is 5.8105 (eV) and the dipole moment μ is 2.0445 (Debye), indicating that this finding will result in strong inhibition efficiency since the energy required to remove an electron from the final occupied orbital will be minimized[45,46] .

HOMO and LUMO are essential factors in chemical reactivity, with HOMO indicating the ability to give an electron and LUMO indicating the ability to acquire an electron. Higher HOMO values indicate a better inhibitory activity with increased adsorption of the inhibitor on the metal surface, whereas low LUMO values indicate the capacity to accept the electron of the molecule[47], which means that the adsorption capacity of the inhibitor increases the metal surface with an increase of E_{HOMO} and a decadence of E_{LUMO}. The frontier molecular orbitals HOMO and LUMO of DAP are displayed in Fig. 8, with HOMO and LUMO values determined and summarized in Table 5. The global hardness (η), the global softness (σ), the absolute electronegativity (χ) the index electrophilicity (ω) and the fraction of transferred electrons (ΔN) are important properties for measuring the molecular stability, reactivity and the capacity of inhibition efficiency of molecules. In this study, all these quantum parameters are in perfect

Table 6 — Calculated quantum chemical parameters of DAP

Quantum chemical parameters	DPA
E_{tot} (eV)	-24884.8617
E_{HOMO} (eV)	-5.9231
E_{LUMO} (eV)	-0.1153
ΔE_{gap}(eV)	5.8105
μ (debye)	2.0445
$\eta_{inh\ (eV)}$	2.9052
σ(eV)	0.3443
χ(eV)	3.0192
ω	1.5507
ΔN	0.6772

Table 5 — Synergistic parameter for the corrosion of XC48 in 0.5 mol.L^{-1} H_2SO_4 solution of Zn^{2+} in presence of DAP

Concentration (mol.L^{-1})	S_θ Tafel method	S_θ EIS method
DPA.10^{-3} + Zn^{2+}.10^{-6}	1.52	1.40
DPA.10^{-3} + Zn^{2+}.10^{-5}	1.08	1.17
DPA.10^{-3} + Zn^{2+}.10^{-4}	1.07	1.02
DPA.10^{-3} + Zn^{2+}.10^{-3}	1.72	1.80

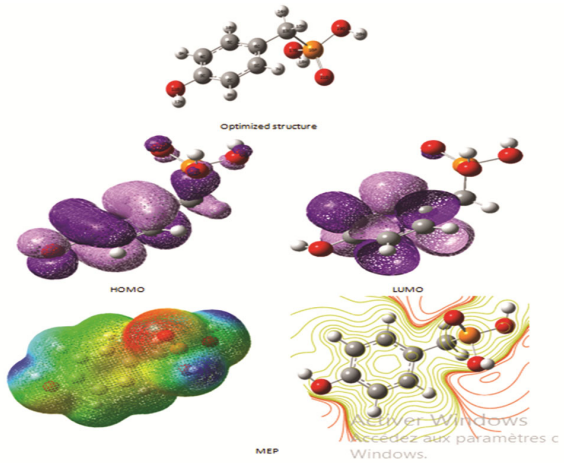

Fig. 8 — Optimized structure, HOMO and LUMO frontier orbitals and MEP map of DAP

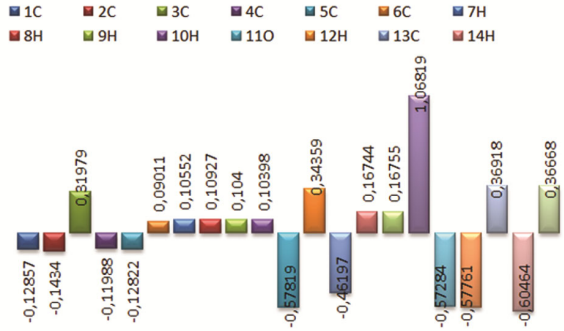

Fig. 9 — Mulliken charge distribution of DAP

The charge distributions over the atoms suggest the formation of donor and acceptor pairs involving the charge transfer in the molecule[48]. The results of calculating Mullikan charges for DAP are listed in Table 6 and Mulliken charge distribution is shown in Fig. 9. According to Table 7, the inhibitors' greater negative charges are found on the O11, O17, O18, and O20 atoms, implying that these atoms are the active adsorptive sites.

The condensed Fukui model indices are employed to investigate the local reactive sites of the inhibitors for nucleophilic and electrophilic attack by finite difference approximation, the condensed Fukui functions can be written as[49,50].

(For nucleophilic attack)

$$f_k^+ = [qk(N+1) - qk(N)] \quad ...(13)$$

(For electrophilic attack)

$$f_k^- = [qk(N) - qk(N-1)] \quad ..(14)$$

where qk(N), qk(N+1) and qk(N-1) are the electronic population of the atom k in neutral, anionic and cationic systems respectively.

The equation Δf *(r)* introduced by Morell *et al.*[51] , is used to calculate the values of the dual descriptor.

Table 7 — Calculated Mullikan and condensed Fukui atomic charges of the studied inhibitor

Atoms	qk(N)	qk(N+1)	qk(N-1)	f_k^+	f_k^-	Δf
1C	-0,12857	-0,25604	-0,07568	-0,12747	0,05289	0,07458
2C	-0,1434	-0,06014	-0,14587	0,08326	0,00247	0,08079
3C	0,31979	0,36828	0,35041	0,04849	-0,03062	0,07911
4C	-0,11988	-0,09388	-0,16724	0,026	0,04736	-0,02136
5C	-0,12822	-0,06536	-0,09125	0,06286	-0,03697	0,09983
6C	0,09011	0,12734	0,09553	0,03723	-0,00542	0,04265
7H	0,10552	0,16745	0,08065	0,06193	0,02487	0,03706
8H	0,10927	0,18415	0,05349	0,07488	0,05578	0,0191
9H	0,104	0,16503	0,03198	0,06103	0,07202	-0,01099
10H	0,10398	0,18698	0,05291	0,083	0,05107	0,03193
11O	-0,57819	-0,58973	-0,43372	-0,01154	0,14447	-0,13293
12H	0,34359	0,37293	0,29703	0,02934	0,04656	-0,01722
13C	-0,46197	-0,48191	-0,41439	-0,01994	-0,04758	0,02764
14H	0,16744	0,19993	0,08161	0,03249	0,08583	-0,05334
15H	0,16755	0,19474	0,09322	0,02719	0,07433	-0,04714
16P	1.068193	1.101130	0.9977020	0,032937	0,070491	0,051714
17O	-0,57284	-0,5485	-0,64588	0,02434	0,07304	-0,0487
18O	-0,57761	-0,53331	-0,6347	0,0443	0,05709	-0,01279
19H	0,36918	0,37156	0,18405	0,00238	0,18513	-0,18275
20O	-0,60464	-0,66599	-0,51999	-0,06135	-0,06135	-0,0233
21H	0,36668	0,37299	0,29252	0,00631	0,07416	-0,06785

agreement with the experimental one.

$$\Delta f(r) = f_k^+ \ - f_k^- \quad ...(14)$$

The highest value of f_k^+ denotes the nucleophilic attack's chosen site, while the highest value of f_k^- shows the electrophilic attack's preferred site. Furthermore, we may detect both sorts of reactive sites concurrently using the $\Delta f(r)$ value. As a result, the nucleophilic assault is advantageous when $\Delta f(r) > 0$, while the electrophilic attack is advantageous when $\Delta f(r) < 0$. Table 7 shows the results of q(N+1), q(N), q(N-1), f_k^+, f_k^-, and $\Delta f(r)$ for the investigated inhibitor. The nucleophilic attack sites are the 1C, 2C, 3C, 5C, 6C, and 13C atoms, while the electrophilic attack sites are the 4C, 11O, 17O, 18O, and 20O atoms, according to these findings.

Conclusion

Potentiodynamic polarization measurements and electrochemical impedance spectroscopy have been used to investigate the synergistic effect of dihydroxy benzyl phosphonic acid (DAP) and zinc sulfate $ZnSO_4$ (Zn^{2+}) system in 0.5 M H_2SO_4 solution on carbon steel X48. The inhibition efficiency increases with the inhibitor concentration, according to the potentiodynamic polarization curves. The addition of Zn^{2+} to H_2SO_4 containing phosphonic acid reveal that efficiency rose with concentration from 73.74to 96.14 percent, implying that DAP and Zn^{2+} has a synergistic effect. The polarization measurements are validated by electrochemical impedance spectroscopy (EIS) tests. The Langmuir isotherm governs the adsorption of DPA and DPA/ Zn^{2+}, and the values of ΔG°ads suggest spontaneous adsorption of the inhibitor on carbon steel surface. The protective film is made up of DAP-Fe^{2+} complex and $Zn(OH)_2$, as shown by FTIR spectra, and SEM micrographs demonstrate the creation of a protective layer on the metal surface. The energies of the highest occupied molecular orbital E_{HOMO} and the lowest unoccupied molecular orbital E_{LUMO}, the energy variation (ΔE_{gap}), the dipole moment (μ), the hardness(η), the softness σ, the electrophilicity ω, the électronégativity χ, and the number of electrons transferred (ΔN) of DAP show that the stydied molecule has a high inhibition efficiency, which is in good agreement with the experimental results presented in this paper.

Acknowledgement

This research is supported by Algerian Ministry of Scientific Research, Laboratory of Electrochemistry of Molecular Materials and Complex (LEMMC), Ferhat Abbas University of Sétif.

References

1 Qiang Y, Zhang S, Xu S, Guo L, Chen N & Obot I B, *Int J Electrochem Sci*, 11 (2016) 3147.
2 Hu L, Zhang S, Li W & Hou B, *Corros Sci*, 52 (2010) 2891.
3 Zheng X, Zhang S, Li W, Gong M & Yin L, *Corros Sci*, 95 (2015) 168.
4 Wang G, Liu S, Wei S, Liu Y, Lian J & Jiang Q, *Sci Rep*, 6 (2016) 1.
5 Kertit S, Aride J, Ben-Bachir A, Sghiri A, Elkholy A & Etman M, *J Appl Electrochem*, 19 (1989) 83.
6 Hegazy M A, Abdallah M & Ahmed H, *Corros Sci*, 52 (2010) 2897.
7 Saker S, Aliouane N, Hammache H, Chafaa S & Bouet G, *Ionics*, 21 (2015) 2079.
8 Amar H, Benzakour J, Derja A, Villemin D, Moreau B & Braisaz T, *Appl Surf Sci*, 252 (2006) 6162.
9 Rajendran S, Apparao B V, Palaniswamy N, Periasamy V & Karthikeyan G, *Corros Sci*, 43 (2001) 1345.
10 Rao S S, Kumar K C, Kiran S R & Diwakar B S, *Mater Today: Procs*, 49 (2022) 588.
11 Kavipriya K, Sathiyabama J, Prabhakar P & Rajendran S, *Chem Sci Trans*, 2 (2012) 570.
12 Amar H, Benzakour J, Derja A, Villemin D, Moreau B, Braisaz T & Tounsi A, *Corros Sci*, 50 (2008) 124.
13 Umamathi T, Arockia Selvi J, Agnesia Kanimozhi S, Rajendran S & John Amalraj A, *Indian J Chem Technol*, 15 (2008) 560.
14 Prabakaran M, Vadivu K, Ramesh S & Periasamy V, *Egypt J Pet*, 23 (2014) 367.
15 Mahmou C, Bouissoui E M, Bouhlal F, Labjar N, Merimi I, Kaya & E l Hajjaji S, *Int J Corros Scale Inhib*, 10 (2021) 1245.
16 Böhmer V, Vogt W, Chafaa S, Meullemeestre J, Schwing M J & Vierling F, *Helv Chim Acta*, 76 (1993) 139.
17 Amin M A, A *Corros Sci*, 52 (2010) 3243.
18 Issa R M, Awad M K & Atlam F M, *Appl Surf Sci*, 255 (2008) 2433.
19 Mahross M H, Efil K, El-Nasr T A & Abbas O A, *J Electrochem Sci Technol*, 8 (2017) 222.
20 Zakaria K, Negm N A, Khamis E A & Badr E A, *J Taiwan Inst Chem Eng*, 61 (2016) 316.
21 Gaussian R A, Frisch M J, Trucks G W, Schlegel H B, Scuseria G E, Robb M A, Cheeseman J R, Scalmani G, Barone V, Mennucci B & Petersson G A, *Wallingford CT*, 121 (2009) 150.
22 Kohn W & Sham L J, *Phys Rev*, 137 (1965) A1697.
23 Arivazhagan M & Subhasini V P, *Spectrochim Acta Part A: Mol Biomol Spectrosc*, 91 (2012) 402.
24 Masoud M S, Ali A E, Shaker M A & Elasala G S, *Spectrochim Acta Part A: Mol Biomol Spectrosc*, 90 (2012) 93.
25 Dennington R, Keith T & Millam J, *GaussView, version 5*, (2009).
26 Chetouani A, Hammouti B, Medjahed K & Mansri A, *Der Pharma Chem*, 3 (2011) 307.
27 Düdükcü M & Avcı G, *Res Chem Intermed*, 41 (2015) 4861.

28 Efremenko E N, Azizov R E, Makhlis T A, Abbasov V M & Varfolomeev S D, *Appl Biochem Microbiol*, 41 (2005) 377.

29 Labjar N, Lebrini M, Bentiss F, Chihib N E, El Hajjaji S & Jama C, *Mater Chem Phys*, 119 (2010) 330.

30 Macdonald D D, *Electrochim Acta*, 51 (2006) 1376.

31 Benali O, Larabi L, Traisnel M, Gengembre L & Harek Y, *Appl Surf Sci*, 253 (2007) 6130.

32 McCafferty E & Hackerman N, *J Electrochem Soc*, 119 (1972) 146.

33 Jeraldin U A M & Santhi R J, *Ann Romanian Soc Cell Biol*, 25 (2021) 17091.

34 Ebenso E E, *Mater Chem Phys*, 79 (2003) 58.

35 Rbaa M, Galai M, E l Faydy M, Lakhrissi Y, Ebn Touhami M, Zarrouk A & Lakhrissi B, *J Mater Environ Sci*, 9 (2018) 172.

36 Palanisamy K & Sekar A, *J Adv Electrochem*, 2 (2016) 126.

37 Prabakaran M, Ramesh S & Periasamy V, *Res Chem Intermed*, 39 (2013) 3507.

38 Amar H, Benzakour J, Derja A, Villemin D, Moreau B, Braisaz T & Tounsi A, *Corros Sci*, 50 (2008) 124.

39 Juribašić M & Tušek-Božić L, *J Mol Struct*, 924 (2009) 66.

40 Rajendran S, Apparao B V, Periasamy V, Karthikeyan G & Palaniswamy N, *Anti-Corros Meth Mater*, 43 (1998) 1345.

41 Cross A D & Jones R A*, Introd Pract Infra Red Spectrosco*, Butterworths, London (1969) 38.

42 Sekine I & Hirakawa Y, *Corros*, 42 (1986) 272.

43 Gomma G K, *Mater Chem Phys*, 55 (1998) 241.

44 Mahross M H, Efil K, El-Nasr T A & Abbas O A, *J Electrochem Sci Technol*, 8 (2017) 222.

45 Becke A, *J Chem Phys*, 98 (1993) 5648.

46 Cano E, Polo J L, La Iglesia A & Bastidas J M, *Adsorption*, 10 (2004) 219.

47 Kikuchi O, *QSAR*, 6 (1987) 179.

48 Pearson R G, *Inorg Chem*, 27 (1988) 734.

49 Musa A Y, Kadhum A A H, Mohamad A B, Rahoma A A B & Mesmari H, *J Mol Struct*, 969 (2010) 233.

50 Lewars E G, *Computational Chem,* Springer, Cham, (2016), 613.

51 Morell C, Grand A, & Toro-Labbé A, *J Phys Chem A*, *109*(1), (2005), 205.